Middle and low latitudes hemispheric asymmetries in ∑O/N2 and TEC during intense magnetic storms of Solar Cycle 24

Waqar Younas, Majid Khan, C. Amory-Mazaudier, Paul O Amaechi, R. Fleury

Journal Pre-proofs

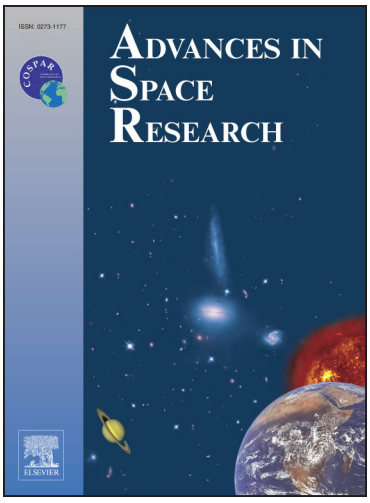

Middle and low latitudes hemispheric asymmetries in ∑O/N2 and TEC during intense magnetic storms of Solar Cycle 24

Waqar Younas, Majid Khan, C. Amory-Mazaudier, Paul O. Amaechi, R. Fleury

PII: S0273-1177(21)00787-0
DOI: https://doi.org/10.1016/j.asr.2021.10.027
Reference: JASR 15563

To appear in: *Advances in Space Research*

Received Date: 5 June 2021
Revised Date: 7 October 2021
Accepted Date: 13 October 2021

Please cite this article as: Younas, W., Khan, M., Amory-Mazaudier, C., Amaechi, P.O., Fleury, R., Middle and low latitudes hemispheric asymmetries in ∑O/N2 and TEC during intense magnetic storms of Solar Cycle 24, *Advances in Space Research* (2021), doi: https://doi.org/10.1016/j.asr.2021.10.027

Middle and low latitudes hemispheric asymmetries in ∑O/N2 and TEC during intense magnetic storms of Solar Cycle 24

Waqar Younas[1], Majid Khan[1], C. Amory-Mazaudier[2, 3], Paul O. Amaechi[4], R. Fleury[5]

[1]Department of Physics, Quaid-i-Azam University Islamabad, Pakistan

[2]Sorbonne Université, Ecole polytechnique, Institut Polytechnique de Paris, Université Paris Saclay, Observatoire de Paris, CNRS, Laboratoire de Physique des Plasmas (LPP), 75005 Paris, France

[3]T/ICT4D, The Abdus Salam International Centre of Theoretical Physics, Italy

[4]Department of Physical Sciences, Chrisland University, Abeokuta, Nigeria

[5]Lab-STICC/CNRS-UMR 6285, IMT-Atlantique, site de Brest, France

*Corresponding author: Dr. Majid Khan (email: majid.khan@qau.edu.pk)

Abstract

We have investigated the global hemispheric differences in thermospheric $\sum O/N_2$ and its impact on the ionospheric total electron content (TEC) at mid- and low-latitudes. Four intense storms of solar cycle 24 (SC-24) have been considered, three of them occurred in Spring equinox and one in Summer solstice season. It is found that the mid-latitudes region has exhibited a large decrease in $\sum O/N_2$ during all the phases of the storms under consideration, which corresponds well to the observed negative storm effects. This decrease is directly related with the storm intensity. The maximum reduction in the $\sum O/N_2$ is observed for the St. Patrick day storm of 2015 (which was the most intense geomagnetic storm of SC-24), whereas the respective minimum decrease is found for the storm of April 2012. Strong hemispheric asymmetries, in $\sum O/N_2$ variation, have been observed at the mid-latitudes sector, and can be associated with the asymmetric energy input as indicated by polar cap (PC) indices. The high speed solar winds streams (HSSWs) during the recovery phases of March 2013 and 2015 storms have caused a significant reduction in $\sum O/N_2$ at mid-latitudes, which could not be reproduced by the coupled thermosphere-ionosphere-plasmasphere electrodynamics (CTIPe) model. On the other hand the low-latitudes region depicts an enhancement in $\sum O/N_2$ during all the storms except for the early recovery phases. The positive storm effect at low-latitudes agrees well with this $\sum O/N_2$ increase, thus indicating that the composition change is one of the major drivers of TEC enhancement at low-latitudes. The CTIPe model showed discrepancies in reproducing the satellite data for all the considered storms, especially during the recovery phases. Furthermore, the model is failed to replicate the hemispheric asymmetries at low and mid-latitudes during the main and early recovery phases.

Key Words

Disturbed $\sum O/N_2$, GUVI/TIMED data, hemispheric asymmetries, REC, CTIPe model

1. Introduction

Ionospheric electronic density changes drastically during the magnetic storms with adverse impacts on ground and satellite based global navigation satellite system (GNSS) communications. The GNSS applications are used in various endeavors including positioning and navigation, search, rescue and geophysical survey. Several mechanisms are responsible for the ionospheric electron density variations during a storm.

The large energy inputs at high-latitudes and Joule heating generate equatorward thermospheric winds and disturbance dynamo electric fields. Storm-time Joule heating leads to the formation of additional pressure gradient from the pole to the equator and an increased neutral density in the upper thermosphere. Due to high-latitude heating and a corresponding increase in the scale heights of all neutral components, the densities of molecular nitrogen and atomic oxygen increase in the upper thermosphere of high latitudes. The excess pressure in the auroral thermosphere changes the wind pattern and a horizontal transfer of air from the auroral to middle and equatorial latitudes is enhanced. In this regard atomic oxygen (lighter gas) is transported faster and farther away from the heating zone in comparison with molecular nitrogen (heavier gas) (Burns et al., 1995; Ratovsky, 2018). Thus, resulting in the observed ionospheric electron density variations. Seaton (1956) proposed that the decrease in ionospheric electron density during a magnetic storm is caused by the composition changes, which was later confirmed by Duncan (1962). Thermospheric neutrals composition changes can be tracked by $\sum O/N_2$ column density ratio. The $\sum O/N_2$ variation in turn is directly proportional to the changes in electron density (Strickland et al., 2001).

Besides storm-time variations in neutral density, there are also quiet-time fluctuations as caused by the solar cycle and season. For example Qian and Soloman (2011) reported the temporal and spatial variation of $\sum O/N_2$. Various trends in temporal variations have been identified such as diurnal, multiday, annual, semi-annual and solar rotation. Thermospheric $\sum O/N_2$ also varies with latitude, longitude and altitude.

Thayer et al. (2008) analyzed the signature of high speed solar winds streams (HSSWs) on thermospheric density during the year 2006 by using the CHAMP data. It was found that the magnitude of thermospheric perturbations, resulted from HSSWs, are not comparable to those associated with large magnetic storms, and relatively long recovery time makes the effects significant. Kil et al. (2011) studied the disturbance in column density during the magnetic storm of November

2003 by using the Global Ultraviolet Imager (GUVI) on board Thermosphere Ionosphere Mesosphere Energetics and Dynamics (TIMED) satellite data. Their results show a positive correlation between ionospheric total electron content (TEC) and thermospheric $\sum O/N_2$ density enhancement. Recently, Yu et al. (2021) studied the altitude profiles of neutral densities during the super storm of November 2003 using GUVI limb data. They concluded that decrease in $\sum O/N_2$ during the main and recovery is mainly attributed to depletion of atomic oxygen in lower thermosphere whereas enhancement in $\sum O/N_2$ is mainly caused by reduction of N_2.

The other storm mechanisms such as prompt penetration electric fields (PPEF) and disturbance dynamo electric fields (DDEF) have also received a considerable attention over the last two decades (Tsurutani et al., 2008; Astafyeva et al., 2016; Astafyeva et al., 2018; Klimenko, 2012; Manoj et al., 2013; Huang, 2013; Abdu, 2016; Hui et al., 2017). However, the present study focuses on quantifying the global hemispheric changes in $\sum O/N_2$ and the associated effects in TEC at the mid and low-latitudes. In this regard, we have also evaluated the capability of the CTIPe model in reproducing the observed features of the variability in $\sum O/N_2$ during various storms in both hemispheric latitudes.

The rest of the article is organized as follows: section 2 describes the data set and the model used while in section 3 we have presented the observed results. In sections 4 and 5, the discussion and conclusions are provided, respectively.

2. Data Sets and Methodology

We have analyzed four geomagnetic storms of varying intensity which observed during solar cycle 24 (SC-24). Table 1 presents various associated parameters as discussed in the following subsections.

2.1 Interplanetary and magnetic parameters

The solar wind parameters, such as speed and Bz component of interplanetary magnetic field (IMF) are provided by ACE satellite and are accessed via the OMNIWEB data center, http://omniweb.gsfc.nasa.gov/.

The magnetic indices, namely auroral electrojet (AE) and symmetric H (SYM-H) are provided by the world data center (WDC) Kyoto, Japan, http://wdc.kugi.kyoto-u.ac.jp. The AE index is used to estimate energy inputs to the ionosphere/magnetosphere system, while the SYM-H index characterizes the strength of a storm by measuring a depression in the magnetic field as caused by diamagnetic ring currents (Wanliss & Showalter, 2006). The energy input to each hemisphere is estimated by the so-

called polar cap (PC) indices (Stauning et al., 2008); polar cap north (PCN) and polar cap south (PCS) indicate energy input to the respective hemisphere.

2.2 Thermospheric ∑O/N_2

Thermospheric variation in ∑O/N_2 data is provided by GUVI spectrometer of the TIMED satellite which was launched by NASA on 06 December 2001. The GUVI spectrometer provides a detailed view of a 2000 km-wide swath in a fixed local time every 100 minutes at an altitude of 625 km. The TIMED satellite precesses at the rate of 3^o per day. Hence, GUVI measurements covers 10-12 LT and 16-18 LT during equinox and solstice seasons, respectively (Zhang et al., 2004; Zhang & Paxton, 2011). GUVI monitors five major airglows bands: H [121.6 nm], OI [130.4 nm & 135.6 nm], Lyma-Birge-Hopfield short (LBHS) band [140-150 nm] and Lyma-Birge-Hopfield long (LBHL) band [165-180 nm]. The altitude range of density profiles is from 110 km to 667 km while beyond 300 km data is extrapolated due to limited sensitivity of dayglow. The OI (135.6 nm) and LBHS dayglow intensities are inverted to produce the altitude profiles of neutral densities and eventually thermospheric O/N2 (Strickland and Evans, 1995; Strickland et al., 1999; Yu et al., 2020). The GUVI data is managed by Johns Hopkins University Applied Physics Laboratory (JHUAPL) and is available at http://guvitimed.jhuapl.edu/data_fetch_l3_on2_idlsave in IDLsave format. The average value of ∑O/N_2 for an orbit over each mid and low-latitudes region can be evaluated as

$$\left\langle \frac{O}{N_2} \right\rangle_i = \frac{1}{n_m} \sum_{n=1}^{n_m} \left(\frac{O}{N_2} \right)_n , \qquad (1)$$

where i denotes the latitudinal geographic limit, namely 0◦:30◦, 0◦: -30◦, 30◦:60◦ and -30◦:-60◦ for northern low-latitudes, southern low-latitudes, northern mid-latitudes and southern mid-latitudes, respectively. The symbol n_m is maximum number of measurements available during each orbit in the respective latitudinal limit. The quiet time average ∑O/N_2 is calculated in the similar way as depicted in Eq. (1) from five quiet days prior to a storm. We can compute the percentage deviation % Δ in storm time ∑O/N_2, from its quiet value, by using the relation

$$\%\,\Delta\left[\frac{O}{N_2}\right] = \frac{Disturbed\left[\frac{O}{N_2}\right] - Quiet\left[\frac{O}{N_2}\right]}{Quiet\left[\frac{O}{N_2}\right]} \times 100 \qquad (2)$$

2.3 Electron content

To analyze the electron content variations at low- and mid-latitudes we have used the UPC Quarter an hour Rapid GIM (UQRG) global ionospheric maps (GIMs) of 15 minutes resolution, as provided by Universitat Politecnica de Catalunya (UPC). The regional electron content (REC) at low and mid–latitudes is computed by using the Afrimovich et al. (2008) method as shown in equation 3.

$$REC = \sum_{m,n} I_{m,n} A_{m,n}\,, \qquad (3)$$

where m and n denote the latitude and longitude of respective GIM cell, I and A are, orderly the TEC value and area of corresponding cell. First, we computed the REC at northern low-latitudes (0◦:30◦N), northern mid-latitudes (30◦:60◦N), southern low-latitudes (0◦:30◦S) and southern mid-latitudes (30◦:60◦S). Then the difference in REC, i.e., ΔREC was calculated by subtracting the respective daily quiet variations.

2.4 CTIPe Model

The coupled thermosphere ionosphere plasmasphere electrodynamics (CTIPe) model (Millward et al., 1996; Millward et al., 2001) is a physics based numerical code developed at the National Oceanic and Atmospheric Administration (NOAA) space weather center. The model is based on the solution of energy, momentum and composition equations. The required input global parameters such as solar wind speed, density and IMF are provided by OMNI web data center, and it uses Wiemer model (Weimer, 2005) for computation of ionospheric electric fields. The CTIPe has four main components: 1) global thermosphere (Fuller-Rowell and Rees, 1980; 1983), 2), high-latitudes ionosphere model (Quegan et al., 1982), 3), low- and mid-latitudes ionosphere model (Bailey, 1983) and 4) and Wiemer electric field model. These components are then coupled with energy, momentum and continuity equations.

We have performed CTIPe model runs remotely at the Coordinated Modeling Center (CCMC). The $\sum O/N_2$ output from the CTIPe is taken along the TIMED track such that the comparisons can be performed on equal footings, and average $\sum O/N_2$ is calculated for the low (0°:30°) and mid (30°:60°) latitudes in a similar way as done for the satellite data.

3. Results

3.1 Case 1: The storm of April 2012

The global geomagnetic parameters for this storm are presented in Fig. 1(a), where from top to bottom we have: IMF Bz in nano tesla (nT), solar wind speed in km/s, AE index in nT, PC indices in mV/m and SYM-H index in nT from 21 to 29 April 2012. The vertical dotted line, in each subfigure, corresponds to the sudden storm commencement (SSC) at 0315 UT on 23 April 2012. Soon after the SSC, IMF Bz turned southward and reached a minimum value of -13.63 nT at 0459 UT. Then it started oscillating and finally turned southward from 1725 UT to 0445 UT on the following day with a minimum IMF Bz value of -15.85 nT. The solar wind speed remained approximately constant around 400 km/s, whereas the AE index reveals several periods of energy input throughout this event with peak values of 1010 nT, 1829 nT, 1015 nT and 1371 nT at 0607 UT 23rd April, 2037 UT 23rd April, 2109 UT 24th April and 1818 UT 25th April, respectively. The PC indices show two episodes of energy input with maximum PCN=7.09 and PCS=7.24mV/m. From the analysis of SYM-H index, we conclude that the main phase of this storm began at 1758 UT on 23rd April and lasted till 0408 UT on 24th April having a minimum value of -123nT, while recovery phase lasted till the end of April 27, 2012.

From top to bottom in Fig. 1(b) we have presented – from 21 to 29 April 2012 – the thermospheric disturbed $\sum O/N_2$ variations (red), quiet $\sum O/N_2$ (blue) and $\Delta\mathrm{REC}$ (black) over the northern hemisphere low-latitudes, southern hemisphere low- latitudes, northern hemisphere mid-latitudes and southern hemisphere mid-latitudes, respectively. At the northern low-latitudes region, there is about 16.2 % enhancement at 0315 UT on April 24, whereas we also observe a degradation of column density by 24.88 % at 1925 UT on the same day. Moreover, the figure also reveals that there is an enhancement of 6% on 26th April, 10.54% on 27 April, 5.33% on 28 April 5.82% on 29th April and 9.29 % on the 30th of April 2012. For the southern low-latitudes we have obtained 14.75%, 7.36%, 15.53%, 7.77%, 4.19% and 9.22% increase in $\sum O/N_2$ on 24th, 25th, 26th, 27th, 28th and 29th of April 2012, respectively. However, at the northern mid-latitudes, there is no significant deviation from respective quite values

except on 24th of April 1800UT where we note a decrease, from the pre-storm value, of 25%. At the southern mid-latitudes, there is 17.15% enhancement during the late hours of 23rd April 2012 and 58.68%, 35.70% decrements, respectively on 24th and 25th of April, whereas the ratio increases by 20.15% on April 26, 2012. The variations in regional electronic current, i.e., $\Delta\mathrm{REC}$ show a negative storm effect at the northern low and mid-latitudes region on 24 (REC: -0.087, -0.089) and 26 April 2012 (REC: -0.067, -0.075). Whereas the southern hemisphere, at low-latitudes, depicts largest positive storm effects with respective REC values of 0.189, 0.156 and 0.138, orderly on 24, 25 and 26th of April 2012. The southern hemisphere mid-latitudes, on the other hand, do not show any significant deviation.

Figure 1(c) shows $\sum O/N_2$ ratio as obtained from GUVI/TIMED (in red) superimposed by the corresponding values evaluated from the CTIPe model run along the TIMED track. Here we note that at the low-latitudes the $\sum O/N_2$ values as predicted by CTIPe model have a higher magnitude than the respective TIMED-GUVI data. Furthermore, the model was unable to reproduce the $\sum O/N_2$ variations at low-latitudes. At mid-latitudes, although there are differences (during the storm) between the model and GUVI data, we find a better agreement for the post storm period.

3.2 Case 2: The storm of March 2013

Figure 2(a) is similar to 1(a) except that it is for the period from 14th March to 25th 2013. The vertical dotted line on 17th March 2013 at 0445UT corresponds to the arrival of a coronal mass ejection (CME). The IMF Bz started oscillating after the SSC, turned southward and remained there till the end of 17th March. The solar wind speed has increased from 428 km/s to 730 km/s and the AE index depicts large energy inputs with a maximum peak of 2690nT at 16.50UT on 17th March 2013. The PC indices show two periods of energy input with maximum PCN and PCS values of 8.7mV/m and 11.25mV/m, respectively, i.e. the southern hemisphere exhibiting a large energy input than its northern counterpart. The SYM-H index depicts a minimum value of -132 nT at 2030UT on 17th March 2013. There are also periods of HSSW during the recovery phase, which starts on 20th March at 1100UT and solar wind speed reached to 683 km/s at 1737UT on the same day.

Figure 2(b) is similar to 2(a) for the period of 14 March to 25 March 2013, it highlights 12.7%, 15.9%, 7%, 7.2% and 10.15% enhancement in $\sum O/N_2$, respectively on 17th, 18th, 19th, 20th and 21st of March 2013 at the low-latitudes of northern hemisphere. Whereas at the corresponding latitudes on

southern hemisphere there is an increase of 17.2% on 17 March 2013 and 35% reduction on 18th of March 2013. This disturbance in $\sum O/N_2$ at the southern low-latitudes lasted till 25th of March 2013 having about 10% enhancement on the days after 18th March 2013. During this space weather event, the $\sum O/N_2$ variation at the mid-latitudes for both hemispheres is found to be symmetric and there is a major episode of $\sum O/N_2$ decrease on 17-18 and 21st March 2013. There is also a decrease of 42%, 24.8%, 11.3%, 21%, 55%, 26.8%, 21.19% and 28.42%, orderly on 17, 18, 19, 20, 21, 22, 23 and 24th day of March 2013 at the northern mid-latitudes. The southern mid-latitudes region has shown 48.7% and 17.60% rise in $\sum O/N_2$ on 18th and 19th March 2013. The ΔREC data exhibit two periods of disturbance in REC, first on the days of storm, i.e. 17th March and second on 21st of March 2013. At low-latitudes (in both hemispheres), there are two episodes of REC enhancement of almost same magnitude on the day of storm, whereas on 18th March a negative storm effect is observed at all the regions except for the northern low-latitudes. The negative storm effect occurred first at the northern mid-latitudes followed by the southern mid- and low-latitudes region, respectively.

In Figure 2(c), we have compared the performance of CTIPe with TIMED satellite data for the storm of March, 2013. The model shows a good agreement at northern low-latitudes while at southern low-latitudes it has failed to reproduce the strong fluctuations on the day after the storm, i.e. 18th March.

3.3 Case 3: The storm of March 2015

This storm – also referred to as St. Patrick day storm – is considered to be the largest geomagnetic event of solar cycle 24 where SYM-H index reached minimum value of -222 nT. In Fig. 3(a) we present different associated global parameters, namely IMF Bz in nT, solar wind speed in km/s, AE index and SYM-H index in nT from 14 to 26 March 2015. The PC indices show a large energy input that lasted till 21st of March 2015. The vertical dotted line on 17th March 2015 at 0445UT corresponds to the arrival of a CME, with IMF Bz performing two major southward excursions on 17th March and an increase in solar wind speed (400 km/s to 630 km/s) is observed. The AE index highlights large auroral activities on 17th and 18th March having the largest peak of 2300 nT.

Using Eq.(1) the $\sum O/N_2$ variations at the low- and mid-latitudes have been calculated for TIMED satellite data and the results are presented in Fig. 3(b). The northern low-latitudes show a large enhancement soon after the CME strike, in particular we note 15.6%, 22.63%, 11.3% and 9.5% increase, respectively on 17th, 18th, 19th and 20th of March. At the southern counterparts, there is an

enhancement (23.78% and 21.59%) in $\sum O/N_2$ ratio on March 17 and 18, which is followed by a decrease (23.33%) on 19th March 2015. The mid-latitudes of both hemispheres have a symmetric response except that in northern (southern) hemisphere disturbance returns to its pre-storm value on 23rd (22nd) March. There is 62% and 45% reduction, respectively on 17th and 18th of March 2015 at the northern mid- latitudes, whereas the corresponding degradation is 59.5% and 58.5% at the southern counterpart. The REC variations during the St. Patrick day storm reveal that there are two positive peaks of almost equal magnitude at all longitudes, which is followed by a smaller peak on 17th of March 2015. The negative storm effect has been first observed at the northern mid-latitudes followed, orderly by northern low-latitudes, southern low- and mid-latitude. A maximum negative storm effect is noted at southern low-latitudes and subsequently at the southern mid-latitude, northern mid- and low-latitudes on 18th of March, which is then seen to decrease slowly and eventually reaches to its pre-storm value on 22nd of March.

Figure 3(c) compares the $\sum O/N_2$ variation as observed for GUVI/TIME with CTIPe model. A careful analysis of both data sets show that the model succeeded well in reproducing the observed data at all the regions excepts at the southern low- latitudes where $\sum O/N_2$ returns to its pre-storm value very quickly.

3.4 Case 4: The storm of August 2018

Figure 4(a) describes the geomagnetic activity during the space weather event of August 2018, here we have (from top to bottom) IMF Bz in nT, solar wind speed in km/s and SYM-H index in nT from 23-30 August 2018. The vertical dotted line corresponds to SSC on 25 August at 0730UT. This event is associated with a long southward directed IMF Bz which turned southward at 1700UT and remained there till 0945UT of the next day (26th of August) and the solar wind speed has increased from 300 km/s to 600 km/s. The PC indices show a large energy input on 26th August having a maximum value of PCS=11.3mV/m in the southern hemisphere. The corresponding SYM-H index reached a minimum value of -206 nT on 26th of August 2018 at 0711UT.

Figure 4(b) is similar to Figure 3(b) from 23rd to 30th of August 2018. It is observed that there is an enhancement in $\sum O/N_2$ ratio at the northern low-latitudes at 26th of August and reaches a maximum at 0700UT with 23% rise. The maximum decrease of 32% is observed at 1950 UT of the same day. Further, there is 16.5%, 14.2% and 10% rise in $\sum O/N_2$ on 27, 28 and 29 august 2018, orderly. On the

other hand the southern low-latitudes show a 16% enhancement only on 26th of August 2018. The northern mid-latitudes depict a large decrease (31.7%) on 26th of August followed by 19.7% and 13.9% decrease on 28 and 29 August 2018, respectively. Whereas the southern mid-latitudes represent a 53% decrease during main phase on 26th august at 0950UT followed by an increase of 28% at 1755UT during recovery phase. Furthermore, there is 47%, 38% and 31.7% degradation in $\sum O/N_2$ on 27th, 28th and 29th of August 2018 at southern mid-latitudes, correspondingly. The ΔREC variations at the four regions during 23 to 30 August 2018 depict a positive storm effect on 26 August having a maximum REC=0.1 at low-latitudes (both hemispheres). The northern hemisphere (mid- and low-latitudes) has shown a negative storm, which has its strongest effect at low-latitudes during the late hours of 26th of August 2018.

Figure 4(c) compares the GUVI/TIMED data with CTIPe model during the storm of August 2018, at the low-latitudes the model predicts a disturbance in $\sum O/N_2$ for the post storm days, whereas at the mid-latitudes there is a large temporal difference with respect to $\sum O/N_2$ changes, i.e. model responded later as compared GUVI data.

3.5 Percentage variation in $\sum O/N_2$ during the storms

Figure 5(a) presents the percentage change in $\sum O/N_2$ from the respective quiet time value calculated using the Eq. (2) for the case of April 2012 at northern low-latitudes (in blue), southern low-latitudes (in red), northern mid-latitudes (in yellow) and southern mid-latitudes (in green) from 21st to 29th of April 2012. From this Figure the low-latitudes region exhibits an enhancement (up to 17% at 0300 UT on 24th April) during the main phase, whereas the mid-latitudes show a decrease in column density, which started earlier in northern hemisphere. On April 22, maximum of 40% and 55% decrease in $\sum O/N_2$ is observed in northern and southern hemisphere mid-latitudes region, respectively. Figure 5(b) is similar to 5(a) for the case of March 2013, namely for a period of 15th to 26th March. The low-latitudes region exhibits an enhancement (up to 20%) on 17th of March, whereas a decrease is observed at the southern low-latitudes stations at 2115UT on 17th and decreased up to 31% at 0340UT on 18th March. The decrease, in observed ratio, in the mid-latitudes started 12 hours earlier in northern hemisphere, whereas the northern and southern mid-latitudes have shown maximum 43% and 51% reduction in $\sum O/N_2$ during the main phase of this storm. The mid-latitudes regions sectors – due to HSSWs – have exhibited a decrease in $\sum O/N_2$ on 21st March with maximum 57% and 39% depletion, respectively in northern and southern regions.

Figure 5(c) is similar to 5(a) for the case of March 2015. The low-latitudes show enhancements in $\sum O/N_2$ on 17th and 18th of the March with maximum increase up to 25% and 29% in northern and southern regions. A decrease in $\sum O/N_2$ which started 05 hours earlier in northern hemisphere is observed at mid-latitudes. The northern hemisphere has shown a maximum of 70% reduction in $\sum O/N_2$, whereas it is 61% for southern mid-latitudes. The northern mid-latitudes have also shown 60% and 51% reduction on 22nd and 23rd of March 2015, as caused by HSSWs.

The percentage change in $\sum O/N_2$ during the case of August 2018 is presented is Fig. 5(d), which revealed that during this space weather event a perturbation in thermospheric $\sum O/N_2$ started around 14 hours after the arrival of the CME. The northern low-latitudes have shown a maximum 22% enhancement at 0830UT on 26th of August, which is followed by a decrease in $\sum O/N_2$, up to 28% at 1950UT. The southern low-latitudes first show a reduction (up to 15% at 1000UT on 26th) in $\sum O/N_2$, followed by a strong enhancement of 45% at 1450 UT. The southern mid-latitudes sector shows a maximum of 54% decrease on 26th of August, which subsequently follow an oscillatory trend and reaches the pre-storm condition on 28th of the August 2018. On the other hand, northern mid-latitudes have depicted a maximum 44% reduction from respective quite time values, recovered gradually and returned to pre-storm value on 28th of August.

4. Discussion

In this section we will discuss the observed hemispheric asymmetries in thermospheric composition changes and its impact on the ionospheric total electron content. At high-latitudes, an upwelling of the polar atmosphere brings N_2 rich air to higher altitudes resulting in a higher loss rates there, and thus the TEC decreases. The maximum decrease in $\sum O/N_2$ occurs in the heating zone i.e., at high latitudes during the disturbed conditions. This negative effect decreases from high to low latitudes and at some latitude, a transition from the negative to positive phase of the $\sum O/N_2$ disturbance is also possible (Ratovsky et al., 2018, Burns et al., 1995). In a recent study by Cai et al. (2020) it is found that the $\sum O/N_2$ disturbance zone can propagate to the low latitudes and stay there for a relatively long duration as compared to high latitudes. The latitudinal boundary of the negative and positive $\sum O/N_2$ disturbances depends on many factors such as season, strength of storm, UT time of commencement and episodes of energy inputs (Fuller-Rowell et al., 1994, 1996). In this regard various first principles models show that (i) negative ionospheric storms at high latitudes are caused by the formation of the N2 thermospheric bulge (Förster et al., 1999; Fuller-Rowell et al., 1994); (ii) compositional

perturbations following the onset of the storm propagate to mid-latitudes due to the advective effects of equatorward winds (Burns et al., 1991); (iii) at low latitudes the positive long-lasting storm-time electron density disturbances can be formed in the daytime due to an increase in the neutral ratio (Field and Rishbeth, 1997; Crowly et al., 2006; Dmitriev et al., 2017; Klimenko et al., 2017, 2018). Fuller-Rowell et al. (1996) showed that the main seasonal effect was in the prevailing summer-to-winter circulation, which transports the composition bulge from the summer polar regions to mid and low latitudes, while in winter, the composition bulge is constrained to remain at high latitudes by the flow from the summer hemisphere. The reduction in TEC at mid-latitudes can be explained in terms of the upwelling that makes the thermosphere richer in N2 and lower in O concentrations, thereby increasing the recombination rate. For the low-latitudes, the downwelling brings the atomic constituents to low altitudes, reducing the loss rate and thus increasing the observed TEC values.

4.1 Mid-latitudes thermosphere $\sum O/N_2$ variations

We have noted a decrease in $\sum O/N_2$ at the mid-latitudes during all the four storms of different intensities, under investigation. This is due to the fact that the enhanced energy input via Joule heating, momentum transfer and particle precipitation at high-latitudes during the magnetic storm generate thermospheric winds that propagate equatorward and also redistribute the nitrogen-rich and oxygen-depleted air at high- and low-latitudes (Seaton, 1956; Prölss, 1980; Strickland et al. 2001; Zang et al., 2004). Thus, it has resulted in the observed reduction in $\sum O/N_2$ from high- to mid-latitudes. Figure 5(a) depicts that during the case of April 2012, there is an increase (about 18%) in $\sum O/N_2$ in the southern mid-latitudes region, whereas a decrease in northern counterpart is observed. During 24th to 27th of April 2012, one finds a large decrease in $\sum O/N_2$ in southern hemisphere at mid-latitudes.

During the case 2, there is a temporal difference in thermospheric $\sum O/N_2$ at mid-latitudes of both hemispheres. The depletion in $\sum O/N_2$ started at 0935UT and 2120UT in northern and southern mid-latitudes sectors, respectively on 17th March 2013 [Fig. 1 (b)]. The maximum decrease -43% (-48.5%) in $\sum O/N_2$ occurred at 2054UT 17th March (0210UT 18th March) in the northern (southern) mid-latitudes. This observed asymmetry at mid-latitudes suggests that energy input at high-latitudes is neither simultaneous nor is of equal strength. The PC index, which is also a proxy of energy input to ionosphere-magnetosphere, shows that the northern hemisphere responded earlier than the southern counterpart. However, it also indicates that southern hemisphere has large energy input (max PCS=11.25mV/m) as compared to northern hemisphere (max PCN=8.69mV/m). For case 2 the hemispheric asymmetries (temporal response and maximum decrease) in the $\sum O/N_2$ changes

correspond to asymmetric energy input to both hemispheres [Förster & Haaland, 2015; Zesta et al., 2016; Laundal et al., 2016; Pakhotin et al., 2021]. The analysis of REC data revealed that the decrease in electron content first started at northern mid-latitudes. The temporal differences in $\sum O/N_2$ depletion at mid-latitudes are also found consistently in total electron content variations at the respective hemisphere. However, there is also a time difference between maximum reduction in $\sum O/N_2$ and maximum negative storm effect, which suggests that $\sum O/N_2$ depletion takes some time to cause the ionospheric density changes. Such hemispheric asymmetry has also been pointed out in a recent statistical study of Ratovsky et al. (2020), where they found that southern hemisphere is more sensitive to geomagnetic storms and is strongly affected by the large-scale physical mechanisms, which drive the disturbances in the thermosphere. Another interesting feature for the case of March 2013 is a large decrease (more than on the day of storm and the day after) in ratio on 21st of March 2013 at northern mid-latitudes, which can be associated to HSSWs event on 21st March as observed in global parameters (Fig. 2b). Thus, we can conclude that HSSWs events can produce disturbance, in thermosphere, which is comparable (in magnitude) to the CME counterparts. Although these HSSWs generated storms generally do not develop strong ring currents, however continuous energy input – due to oscillatory IMF Bz – during these events results into a significant disturbance in the thermosphere. Chen et al., (2014) performed a statistical analysis on the impact of CME and HSSW events on the thermosphere and ionosphere. They concluded that HSSWs can generate thermospheric density variations comparable or even greater than CME counterparts. These HSSWs generated disturbance can also be observed in REC data of mid-latitudes, where depletion in column density is more intense in the northern hemisphere. The CTIPe model shows a reduction in $\sum O/N_2$ during the main and early recovery phases, which agrees with GUVI/TIMED data, however this model depicts a lesser decrease as compared to the experimental data. Moreover, the model is unable to reproduce the large decrease – as caused by HSSWs – in $\sum O/N_2$ on 21st March.

For the magnetic storm of March 2015, the reduction in $\sum O/N_2$ ratio has reached up-to 65% in northern hemisphere on the storm day, whereas southern mid- latitudes show a 55% decrease on the day after the storm as observed in Fig. 5(c). However, the recovery started much earlier (10 hours) in the northern mid-latitudes as compared to corresponding southern hemisphere. This relatively long duration of reduced $\sum O/N_2$ has significantly affected the REC in southern mid-latitudes. The REC data illustrate that the depletion in electron content first started in northern mid-latitudes, however the southern counterparts show a large decrease in electron content. Thus, as relatively long duration of

reduced $\sum O/N_2$ has caused a strong negative storm effect at the southern mid-latitudes. The PC indices also indicate that the southern hemisphere has strong energy input (PCS=11.34mV/m) as compared to the northern region (PCN=8.5mV/m), which causes a strong reduction in $\sum O/N_2$ as well as a negative storm effect in the southern hemisphere. Due to streams of high speed solar wind during the recovery phase we can see a strong decrease in $\sum O/N_2$ ratio in northern hemisphere on 22nd and 23rd of March 2015. This is also in agreement with the findings of Ratovsky et al. (2020) which states that southern hemisphere is more favorable for storm time driving mechanisms. The CTIPe model also produces a decrease in ∑O/N2 at mid-latitudes of both hemispheres during the main and early recovery phases, however it responded later than the observed values. Similar to case 2, CTIPe was unable to capture HSSWs induced reduction in $\sum O/N_2$ ratio on 22nd and 23rd of the March 2015

During the case 4, the reduction in ∑O/N2 is observed almost simultaneously at the start of 26th August 2018 in mid-latitudes region of both hemispheres. The northern mid-latitudes show a maximum of 31% reduction at 0050UT on 27th August, whereas in the southern mid-latitudes sector the maximum depletion reached up to 40% at 0815UT on 25th August 2018. However, recovery started much earlier in the southern hemisphere than the northern counterpart. Furthermore, there is a surprising 26% enhancement in ∑O/N2 at southern mid-latitudes, which is contrary to all of the previous cases, where we did not find any increase at mid-latitudes during the recovery phases. On the other hand, a very slow recovery in ∑O/N2 is observed at the northern hemisphere when the disturbance returns to its quiet time value around 0900 UT on 28th August 2018. This long duration of reduction in ∑O/N2 ratio at northern mid-latitudes has caused a negative storm effect as seen in Fig. 4(d), which is consistent with the results recently reported by Younas et al. (2020) and Astafyeva et al. (2020). The CTIPe model has produced the reduction in ∑O/N2 only at northern mid-latitudes, moreover it is unable to show the enhancement in ∑O/N2 in southern at mid-latitudes during the recovery phase.

For the cases 3 and 4, we observe transitions from negative to positive storm effects (in REC and ∑O/N2) during the recovery phase at mid-latitudes. This is due to the development of additional poleward gradient, which transports the atomic oxygen from low to mid-latitudes and thus decreasing temperature and N2 concentration, i.e. Hence, resulting in the positive storm effects in REC and ∑O/N2. However, this effect is not evident for all cases as it depends on many factors such as strength, intensity and duration of a geomagnetic storm (Ratovsky et al., 2018).

4.2 Low-latitudes thermosphere ∑O/N2 variations

The low-latitudes thermosphere show, mainly, an enhancement in ∑O/N2 during all the considered magnetic storms. For the case of April 2012 southern low-latitudes have exhibited a comparatively large enhancement in ∑O/N2 ratio on 24th and 27th of April [Fig. 5], which corresponds well to the positive storm effect in the respective regions. The simultaneous enhancement in ∑O/N2 and REC in southern low-latitudes suggests that composition enhancement is one of the major drivers of low-latitudes positive storm effect (Balan et al., 2009; Lu et al., 2001; Horvath & Lovell, 2015).

During the case of March 2013, there is an enhancement in column density on all days after the storm except on 18th March where we find a large decrease in southern low-latitudes. The maximum decrease in southern low-latitudes occurred on 18th March at 0340UT (about 1.5 hour later from mid-latitudes). This reduction is attributed to the storm time generated thermospheric winds which were strong enough in southern hemisphere to cause a disturbance at low-latitudes. Furthermore, there is a rise in ∑O/N2 soon after the SSC at the low-latitudes. However, the strong equatorward flowing disturbed winds inhibits this pole-ward expansion of plasma (Yue at al., 2016; Habarulema et al., 2017). The northern mid-latitudes have exhibited a strong enhancement in ∑O/N2 on 17th and 18th March which returned to its pre-storm value on March 25, 2013. The HSSWs on 21st March have significantly reduced the mid-latitudes ∑O/N2 ratio and did not affect the low-latitudes thermosphere. These thermospheric compositions changes also affect the low-latitudes ionization. The corresponding REC data show that the northern low-latitudes exhibit a positive storm effect on all days after the storm which is consistent with the observed thermospheric composition changes. The southern low-latitudes show a negative storm effect on 18th of March and are consistent to the large decrease in ∑O/N2 ratio (Balan et al., 2009; Lu et al., 2001; Horvath & Lovell, 2015; Cai et al., 2020).

During St. Patrick day storm of 2015, there are three peaks of ∑O/N2 enhancement at low-latitudes of both hemisphere on 17th, 18th and 19th of March. The REC data highlights a positive storm effect at low-latitudes in both hemispheres on 17th of March. For this storm, CTIPe is unable to reproduce the storm time changes in thermosphere. During the case of August 2018, the northern hemisphere in the low-latitudes sector depicts a comparatively large rise in thermospheric (Fig. 5 d), which started at 1320UT and reaches to a minimum value at 1950UT on the 26th of August. The low-latitudes REC analysis exhibits a positive storm effect in both hemispheres during the main phase, with almost equal magnitude, however the northern low-latitudes depict a negative storm effect during the late hours of 26th August 2018 at the same time when reduction in ∑O/N2 ratio was observed. This is also

an indicator that low composition is a major driver of TEC changes (Balan et al., 2009; Astafyeva et al., 2020). The CTIPe model has reproduced the storm-time variation in ∑O/N2 except that it was unable to duplicate the rapid variations during the early recovery phase at low-latitudes. Furthermore, the model could not detect the observed compositional changes during the HSSWs.

Our analysis leads to the conclusion that strong hemispheric asymmetries in ∑O/N2 exist – both at mid and low latitudes – during all the storms under consideration. However, the pattern of asymmetry varies from storm to storm and depends on many factors such as asymmetric energy inputs, season, intensity and duration of the storm. For example, during the case of August 2018, northern low latitudes have exhibited about 07% more increase in ∑O/N2 as compared to the southern counterparts. Astafyeva et al. (2020) also reported the hemispheric asymmetries in neutral mass density distributions and ionospheric plasma during the main and recovery phases for the same storm. They submitted that such asymmetries are driven by the combination of mechanisms, which depended on the time, location and asymmetry in the geomagnetic field. Furthermore, the positive enhancement in ∑O/N2 at mid-latitudes is only found in the southern hemisphere. Ratovsky (2018) reported that such rise in ∑O/N2 is due to poleward transport of atomic Oxygen from equatorial and low latitudes. However, our study shows that this mechanism is also not symmetric in both hemispheres. During the case of March 2013, we observe a decrease in ∑O/N2 at low-latitudes during the main phase in the northern hemisphere and a positive increase at mid-latitudes in southern hemisphere. In a similar analysis Bruinsma et al. (2006) attributed the asymmetry, in density during the storm of 20–21 November 2003, to the hemispheric difference in the conductivities that facilitate the flow of ionospheric currents. Dashora et al. (2019) studied the interhemispheric asymmetry in low-latitude TEC during 7 major and 30 moderate ionospheric storms from years 2000–2018. They found that the interhemispheric asymmetry varied from one storm to another and depended on presence of episodic E × B drift and large scale TIDs. They nonetheless suggested that the cause of asymmetry needed further investigation.

4.3 On the accuracy of the model

Table 2 presents the deviation of model generated thermospheric ∑O/N2 from the corresponding satellite data. In this regard the maximum deviation (σ_m) is calculated by difference in CTIPe and GUVI generated % Δ[∑O/N2], the values $\sigma_m \geq 25$ are considered to be significant and are highlighted. It can be observed from the table that model behaves well during magnetic quiet days at low- and mid-

latitudes for all the selected events. During this period the forcing of high-latitudes is weak (Padatella et al.,2018) and CTIPe simulations show only a small deviation (σ_m < 25). During the early hours of the main phase, there is more deviation at mid-latitudes as compared to lower counterparts. In this regard, the maximum deviation is observed for case 3, with σ_m =30 and 40, respectively for northern and southern hemisphere. Here the forcing of high-latitudes is strong and only PPEF is acting at mid-latitudes, this electric field is the main factor responsible for the observed deviations. In the recovery phase there are discrepancies between observed and CTIPe simulated data, for all the four cases at mid-latitudes, which is more prominent for the cases 2 and 4. During this period, the forcing of high-latitudes – due to DDEF and thermal expansion of atmosphere – is strong and is a probable reason of the observed strong deviation during a recovery phase.

Padatella et al. (2018) indicated that uncertainties in equatorial electric field, neutral winds and neutral composition are the major factors affecting the performance of various models – the Thermosphere-Ionosphere-Electrodynamics General Circulation Model (TIE-GCM) in their case and the CTIPe in present study – in the low- and mid-latitudes. They argued that numerical models do not often take into consideration the variability of high-latitude forcing parameters including electric potential/electric field and auroral particle precipitation. In our case we traced the inability of the CTIPe to accurately capture the hemispheric asymmetry in ∑O/N2, during the considered storms, to its misrepresentation of storm time energy input related with polar cap potentials in both hemispheres as well as the nature of solar disturbance, e.g. the presence of HSSWs. In line with the suggestion of Padatella et al. (2018) that the relative contribution of the sources of errors due to high-latitude forcing may vary from one storm to the other, we found that the performance of the CTIPe changes significantly for different storms. For example during the recovery phases of March 2013 and 2015 storms, when there were HSSWs, the model clearly failed to capture the considerable reduction in ∑O/N2 at mid-latitudes.

5. Conclusion

We have studied the thermospheric ∑O/N2 at mid- and low-latitudes during the four magnetic storms of solar cycle 24. In this regard, the roles of disturbed ∑O/N2 in positive/negative storms of ionosphere have been investigated. It is found that the storm time disturbed ∑O/N2 plays a significant role in positive/negative storms at mid and low-latitudes region. The main findings of present study are summarized as follows:

1. Mid-latitudes sector shows a decrease in ∑O/N2 whose amplitude varies with the strength of a storm during all events under consideration. However, during the St. Patrick day storm of 2015, the depletion in thermospheric composition ratio has reached to 65% from the pre-storm value in the northern hemisphere.
2. The REC data analysis at the mid-latitudes exhibits the hemispheric asymmetries in the composition changes. A large decrease in ∑O/N2 at the mid-latitudes is a major driver of the associated negative storm effect. Differences in strength and the temporal response of ∑O/N2 reduction are well correlated with the asymmetric energy input.
3. The negative storm effect in REC at mid- latitude has been driven by the observed large decrease in ∑O/N2. Furthermore, there is an observed hemispheric asymmetry in both REC and composition change. This trend is also correlated with the asymmetric energy input as indicated by the PC indices.
4. The Low-latitudes have shown enhancement in ∑O/N2 ratio during all the storms except for a short time reduction during the early recovery phase. The maximum enhancement is found to be strongly dependent on the storm-strength and it ranges between 20 - 25 %. Besides that, the REC enhancement follows the trend of ∑O/N2 and hence indicating that low-latitude composition changes are one of the main drivers of positive storm effects. Moreover, the negative storm effect at the low-latitudes region agrees with ∑O/N2 depletion in the corresponding sectors.
5. During the events of March 2013 and 2015 in southern low-latitudes and for the case of August 2018 in the northern low-latitudes, we observe – only on the day after the storm – a decrease in ∑O/N2 and a corresponding negative storm effect in REC. This depletion indicates that the disturbed ∑O/N2 reaches to the low-latitudes during the period of intense energy input at high-latitudes.
6. The HSSWs, which occurred during the recovery phase of the March 2013 and 2015 storms, are found to cause a depletion in ∑O/N2 at mid-latitudes and its magnitude is comparable to the corresponding values in the main and early phases.
7. The CTIPe model generated ∑O/N2 ratio is found to have higher values during the quiet time. The model has reproduced the observed trends at mid-latitudes but could not capture the rapid changes during the early recovery phase. In particular, the said model is failed to reproduce the large decrease in ∑O/N2 during the recovery phase of the March 2013 and 2015 storms.

8. For all the considered events, especially during the recovery phases, there are discrepancies between GUVI observations and CTIPe predictions. The forcing from high-latitudes in the form neutral winds and DDEF are the possible factors responsible for the observed deviation during a recovery phase.

Acknowledgement

The authors are thankful to the IGS community for making available GNSS data (https://www.igs.org/), OMNI web data center (http://omniweb.gsfc.nasa.gov/) for making available solar wind parameters and geomagnetic activity indices, TIMED/GUVI management team (http://guvitimed.jhuapl.edu/) for providing thermospheric ∑O/N2 ratio. We would like to thank the community coordinated modelling center (CCMC) for making it possible to run coupled thermosphere ionosphere plasmasphere electrodynamics (CTIPe) remotely on request (http://ccmc.gsfc.nasa.gov). The CCMC is a multiagency partnership between NASA, AFMC, AFOSR, AFRL, AFWA, NOAA, NSF, and ONR. W. Younas thanks to L. Rastätter from CCMC, NASA Goddard Space Flight Center, Greenbelt, MD, USA for coordinating in conducing CTIPe model runs. C. Amory-Mazaudier thanks the ISSI-Bern International Team of ‘‘Why Ionospheric Dynamics and Structure Behave Differently in The African Sector?’’ (the team leaders E. Yizengaw & K. Groves) for valuable discussion on part of the results included in this paper.

References

Abdu, M. A. (2016). Electrodynamics of ionospheric weather over low latitudes. Geoscience Letters, 3(1). https://doi.org/10.1186/s40562-016-0043-6

Afraimovich, E. L., Astafyeva, E. I., & Zhivetiev, I. V. (2006). Solar activity and global electron content. Doklady Earth Sciences, 409(2), 921–924. https://doi.org/10.1134/s1028334x06060195

Astafyeva, E., Zakharenkova, I., & Alken, P. (2016). Prompt penetration electric fields and the extreme topside ionospheric response to the June 22–23, 2015 geomagnetic storm as seen by the Swarm constellation. Earth, Planets and Space, 68(1). https://doi.org/10.1186/s40623-016-0526-x

Astafyeva, E., Zakharenkova, I., Hozumi, K., Alken, P., Coïsson, P., Hairston, M. R., & Coley, W. R. (2018). Study of the Equatorial and Low-Latitude Electrodynamic and Ionospheric Disturbances During the 22–23 June 2015 Geomagnetic Storm Using Ground-Based and Spaceborne Techniques. Journal of Geophysical Research: Space Physics, 123(3), 2424–2440. https://doi.org/10.1002/2017ja024981

Astafyeva, E., Bagiya, M. S., Förster, M., & Nishitani, N. (2020). Unprecedented Hemispheric Asymmetries During a Surprise Ionospheric Storm: A Game of Drivers. Journal of Geophysical Research: Space Physics, 125(3). https://doi.org/10.1029/2019ja027261

Balan, N., Alleyne, H., Otsuka, Y., Vijaya Lekshmi, D., Fejer, B. G., & McCrea, I. (2009). Relative effects of electric field and neutral wind on positive ionospheric storms. Earth, Planets and Space, 61(4), 439–445. https://doi.org/10.1186/bf03353160

Bailey, G. J. (1983). The effect of a meridional E × B drift on the thermal plasma at L = 1.4. Planetary and Space Science, 31(4), 389–409. https://doi.org/10.1016/0032-0633(83)90154-x

Bruinsma, S., J. M. Forbes, R. S. Nerem, and X. Zhang (2006), Thermosphere density response to the 20–21 November 2003 solar and geomagnetic storm from CHAMP and GRACE accelerometer data, J. Geophys. Res., 111, A06303, doi:10.1029/2005JA011284.

Burns, A.G., Killeen, T.L., Deng, W., Carignan, G.R., Roble, R.G. Geomagnetic storm effects in the low- and middle-latitude upper thermosphere. J. Geophys. Res. 1995, 100(A8), 14,673-14,691. https://doi.org/10.1029/94JA03232.

Cai, X., Burns, A.G., Wang, W., Qian, L., Solomon, S.C., Eastes, R.W., et al. The two-dimensional evolution of thermospheric ∑O/N2 response to weak geomagnetic activity during solar-minimum observed by GOLD. Geophys. Res. Lett. 2020, 47, e2020GL088838. https://doi.org/10.1029/2020GL088838.

Chen, G., Xu, J., Wang, W., & Burns, Alan. G. (2014). A comparison of the effects of CIR- and CME-induced geomagnetic activity on thermospheric densities and spacecraft orbits: Statistical studies. Journal of Geophysical Research: Space Physics, 119(9), 7928–7939. https://doi.org/10.1002/2014ja019831

Dashora, N., Suresh, S., & Niranjan, K. (2019). Interhemispheric asymmetry in response of low-latitude ionosphere to perturbation electric fields in the main phase of geomagnetic storms. Journal of Geophysical Research: Space Physics, 124, 7256–7282.

Elvira Astafyeva, Mala Bagiya, Matthias Förster, Nozomu Nishitani. Unprecedented Hemispheric Asymmetries During a Surprise Ionospheric Storm: A Game of Drivers. Journal of Geophysical Research Space Physics, 2020, 125 (3), 10.1029/2019JA027261.

Kil, H., Kwak, Y.-S., Paxton, L. J., Meier, R. R., & Zhang, Y. (2011). O and N2 disturbances in the F region during the 20 November 2003 storm seen from TIMED/GUVI. Journal of Geophysical Research: Space Physics, 116(A2), https://doi.org/10.1029/2010ja016227

Klimenko, M. V., & Klimenko, V. V. (2012). Disturbance dynamo, prompt penetration electric field and overshielding in the Earth's ionosphere during geomagnetic storm. Journal of Atmospheric and Solar-Terrestrial Physics, 90–91, 146–155. https://doi.org/10.1016/j.jastp.2012.02.018

Laundal, K. M., Cnossen, I., Milan, S. E., Haaland, S. E., Coxon, J., Pedatella, N. M., et al. (2016). North–South Asymmetries in Earth's Magnetic Field. Space Science Reviews, 206(1–4), 225–257. https://doi.org/10.1007/s11214-016-0273-0

Lu, G., Richmond, A. D., Roble, R. G., & Emery, B. A. (2001). Coexistence of ionospheric positive and negative storm phases under northern winter conditions: A case study. Journal of Geophysical Research: Space Physics, 106(A11), 24493–24504. https://doi.org/10.1029/2001ja000003

Lu, G., Richmond, A. D., Lühr, H., & Paxton, L. (2016). High-latitude energy input and its impact on the thermosphere. Journal of Geophysical Research: Space Physics, 121(7), 7108–7124. https://doi.org/10.1002/2015ja022294

Duncan, R. A. (1969), F-region seasonal and magnetic storm behavior, J. Atmos. Terr. Phys., 31, 59.

Fuller-Rowell, T. J., & Rees, D. (1980). A Three-Dimensional Time-Dependent Global Model of the Thermosphere. Journal of the Atmospheric Sciences, 37(11), 2545–2567. https://doi.org/10.1175/1520-0469(1980)037<2545:atdtdg>2.0.co;2

Fuller-Rowell, T. J., & Rees, D. (1983). Derivation of a conservation equation for mean molecular weight for a two-constituent gas within a three-dimensional, time-dependent model of the thermosphere. Planetary and Space Science, 31(10), 1209–1222. https://doi.org/10.1016/0032-0633(83)90112-5

Förster, M., & Haaland, S. (2015). Interhemispheric differences in ionospheric convection: Cluster EDI observations revisited. Journal of Geophysical Research: Space Physics, 120(7), 5805–5823. https://doi.org/10.1002/2014ja020774

Habarulema, J. B., Katamzi, Z. T., Yizengaw, E., Yamazaki, Y., & Seemala, G. (2016). Simultaneous storm time equatorward and poleward large-scale TIDs on a global scale. Geophysical Research Letters, 43(13), 6678–6686. https://doi.org/10.1002/2016gl069740

Huang, C. M. (2013). Disturbance dynamo electric fields in response to geomagnetic storms occurring at different universal times. Journal of Geophysical Research: Space Physics, 118(1), 496–501. https://doi.org/10.1029/2012ja018118

Hui, D., Chakrabarty, D., Sekar, R., Reeves, G. D., Yoshikawa, A., & Shiokawa, K. (2017). Contribution of storm time substorms to the prompt electric field disturbances in the equatorial ionosphere. Journal of Geophysical Research: Space Physics, 122(5), 5568–5578. https://doi.org/10.1002/2016ja023754

Horvath, I., & Lovell, B. C. (2015). Positive and negative ionospheric storms occurring during the 15 May 2005 geomagnetic superstorm. Journal of Geophysical Research: Space Physics, 120(9), 7822–7837. https://doi.org/10.1002/2015ja021206

Mayr, H. G., and H. Volland (1972). Magnetic storm effects in the neutral composition, Planet. Space Sci., 20, 379

Manoj, C., Maus, S., & Alken, P. (2013). Long-period prompt-penetration electric fields derived from CHAMP satellite magnetic measurements. Journal of Geophysical Research: Space Physics, 118(9), 5919–5930. https://doi.org/10.1002/jgra.50511

Millward, G. R. Moffett, S. Quegan, T. Fuller-Rowell (1996). A coupled thermosphere-ionosphere-plasmasphere model (CTIP), STEP Handbook on Ionospheric Models, pp. 239-279

Millward, G. H., Müller-Wodarg, I. C. F., Aylward, A. D., Fuller-Rowell, T. J., Richmond, A. D., & Moffett, R. J. (2001). An investigation into the influence of tidal forcing on Fregion equatorial vertical ion drift using a global ionosphere-thermosphere model with coupled electrodynamics. Journal of Geophysical Research: Space Physics, 106(A11), 24733–24744. https://doi.org/10.1029/2000ja000342

Pedatella, N. M., Lu, G., & Richmond, A. D. (2018). Effects of high-latitude forcing uncertainty on the low-latitude and midlatitude ionosphere. Journal of Geophysical Research: Space Physics, 123, 862–882. https://doi.org/10.1002/2017JA024683

Pakhotin, I. P., Mann, I. R., Xie, K., Burchill, J. K., & Knudsen, D. J. (2021). Northern preference for terrestrial electromagnetic energy input from space weather. Nature Communications, 12(1). https://doi.org/10.1038/s41467-020-20450-3

Prölss, G. W. (1980), Magnetic storm associated perturbations of the upper atmosphere: Recent results obtained by satellite-borne gas analyzers, Rev. Geophys., 18, 183, https//doi.org/10.1029/RG018i001p00183.

Prölss, G. W. (1981), Latitudinal structure and extension of the polar atmospheric disturbance, J. Geophys. Res., 86, 2385–2396, doi:10.1029/JA086iA04p02385.

Prölss, G. W. (1982), Perturbation of the low-latitude upper atmosphere during magnetic substorm activity, J. Geophys. Res., 87, 5260–5266, doi:10.1029/JA087iA07p05260.

Prölss, G. W. (1993), On explaining the local time variation of ionospheric storm effects, Ann. Geophys., 11, 1–9.

Ratovsky, K. G., Klimenko, M. V., Yasyukevich, Y. V., Klimenko, V. V., & Vesnin, A. M. (2020). Statistical Analysis and Interpretation of High-, Mid- and Low-Latitude Responses in Regional Electron Content to Geomagnetic Storms. Atmosphere, 11(12), 1308. https://doi.org/10.3390/atmos11121308

Ratovsky, K.G., Klimenko, M.V., Klimenko, V.V., Chirik, N.V., Korenkova, N.A., Kotova, D.S. (2018) After-effects of geomagnetic storms: statistical analysis and theoretical explanation. Solar Terrestrial Physics, 4, 26-32. https://doi.org/10.12737/stp-44201804.

Rishbeth, H. (1998), How the thermospheric circulation affects the ionosphere, J. Atmos. Sol. Terr. Phys., 60, 1385–1402, doi:10.1016/S1364-6826(98)00062-5.

Seaton, M. J. (1956), A possible explanation of the drop in F-region critical densities accompanying major ionospheric storms, J. Atmos. Terr. Phys., 8, 122.

Stauning, P., Troshichev, O., & Janzhura, A. (2008). The polar cap (PC) indices: Relations to solar wind parameters and global magnetic activity. Journal of Atmospheric and Solar-Terrestrial Physics, 70(18), 2246–2261. https://doi.org/10.1016/j.jastp.2008.09.028

Strickland, D. J., R. E. Daniell, and J. D. Craven (2001), Negative ionospheric storm coincident with DE-1 observed thermospheric disturbance on October 14, 1981, J. Geophys. Res., 106, 21, 049.

Tsurutani, B. T., Verkhoglyadova, O. P., Mannucci, A. J., Saito, A., Araki, T., Yumoto, K., et al. (2008). Prompt penetration electric fields (PPEFs) and their ionospheric effects during the great magnetic storm of 30-31 October 2003. Journal of Geophysical Research: Space Physics, 113(A5), https://doi.org/10.1029/2007ja012879

Thayer, J. P., Lei, J., Forbes, J. M., Sutton, E. K., & Nerem, R. S. (2008). Thermospheric density oscillations due to periodic solar wind high-speed streams. Journal of Geophysical Research: Space Physics, 113(A6), https://doi.org/10.1029/2008ja013190

Qian, L., & Solomon, S. C. (2011). Thermospheric Density: An Overview of Temporal and Spatial Variations. Space Science Reviews, 168(1–4), 147–173. https://doi.org/10.1007/s11214-011-9810-z

Quegan, S., Bailey, G. J., Moffett, R. J., Heelis, R. A., Fuller-Rowell, T. J., Rees, D., & Spiro, R. W. (1982). A theoretical study of the distribution of ionization in the high-latitude ionosphere and the plasmasphere: first results on the mid-latitude trough and the light-ion trough. Journal of Atmospheric and Terrestrial Physics, 44(7), 619–640. https://doi.org/10.1016/0021-9169(82)90073-3

Wanliss, J. A., & Showalter, K. M. (2006). High‐resolution global storm index: Dst versus SYM‐H. Journal of Geophysical Research, 111, A02202. https://doi.org/10.1029/2005JA011034

Weimer, D. R. (2005). Predicting surface geomagnetic variations using ionospheric electrodynamic models. Journal of Geophysical Research, 110(A12). https://doi.org/10.1029/2005ja011270

Younas, W., Amory-Mazaudier, C.,Khan, M., & Fleury, R. (2020). Ionospheric and magnetic signatures of a space weather event on 25–29 August 2018: CME and HSSWs. Journal of Geophysical Research: Space Physics, 125, e2020JA027981. https://doi.org/10.1029/2020JA027981

Yu, T., Ren, Z., Yu, Y., Yue, X., Zhou, X., & Wan, W. (2020). Comparison of reference heights of O/N2 and ∑O/N2 based on GUVI dayside limb measurement. Space Weather, 18, e2019SW002391. https://doi.org/10.1029/2019SW002391

Yu, T., Wang, W., Ren, Z., Yue, J., Yue, X., & He, M. (2021). Middle-low latitude neutral composition and temperature responses to the 20 and 21 November 2003 superstorm from GUVI dayside limb measurements. Journal of Geophysical Research: Space Physics, 126, e2020JA028427. https://doi.org/10.1029/2020JA028427

Yue, X., Wang, W., Lei, J., Burns, A., Zhang, Y., Wan, W., Liu, L., Hu, L., Zhao, B., & Schreiner, W.S. (2016). Long-lasting negative ionospheric storm effects in low and middle latitudes during the recovery phase of the 17 March 2013 geomagnetic storm. Journal of Geophysical Research: Space Physics, 121(9), 9234–9249. https://doi.org/10.1002/2016ja022984

Zhang, Y., Paxton, L.J., Morrison, D., Wolven, B., Kil, H., Meng, C.-I., Mende, S.B., & Immel, T.J. (2004). O/N2 changes during 1–4 October 2002 storms: IMAGE SI-13 and TIMED/GUVI observations. J. Geophys. Res. 109, A10308, http://dx.doi.org/ 10.1029/2004JA010441.

Zhang, Y., & Paxton, L. J. (2011). Long-term variation in the thermosphere: TIMED/GUVI observations. Journal of Geophysical Research: Space Physics, 116(A2), n/a-n/a. https://doi.org/10.1029/2010ja016337

Zesta, E., Boudouridis, A., Weygand, J. M., Yizengaw, E., Moldwin, M. B., & Chi, P. (2016). Interhemispheric Asymmetries in Magnetospheric Energy Input. In Ionospheric Space Weather (pp. 1–20). John Wiley & Sons, Inc. https://doi.org/10.1002/9781118929216.ch1

Table Caption

Table 1: The details of consider geomagnetic storms depicting the source and minimum of SYM-H Indices.

Table 2: The performance of CTIPe model in reproducing thermospheric O/N_2.

Figure Captions

Figure 1: a) Global parameters, from top to bottom, IMF Bz in nT, solar wind speed in km/s, AE index in nT and SYM-H index in nT from 21st to 29th of the April 2012. **b)** Disturbed thermospheric O/N2 (in red) as obtained by TIMED/GUVI satellite with daily quite variation (in blue) and $\Delta\mathrm{REC}$ (in black), from top to bottom, low-latitudes north (0°:30°N), low-latitudes south (0°: 30° S), mid-latitudes north (0°: 30°N) and mid-latitudes (0°:30°S) from 21st to 29th of April 2012. **c)** Average O/N2 as obtained by TIMED/GUVI (in blue) and corresponding values as generated by CTIPe model, from top to bottom, northern low-latitudes, southern low-latitudes, northern mid-latitudes and southern mid-latitudes during 21-29 April 2012. d) REC at four latitudinal regions from 21st to 29th of April 2012.

Figure 2: a) Similar to Fig. 1(a) but from 14th to 26th of March 2103. **b)** similar to Fig. 1(b) but for the period 14-26 of March 2013. **c)** similar to Fig. 1(c) but from 14 to 26 March 2013.

Figure 3: a) Same as in Fig. 1(a) but from 14th to 26th of March 2015. **b)** similar to Fig. 1(b) but for the period 14-26 of March 2015. **c)** similar to Fig. 1(c) but from 14 to 26 March 2015.

Figure 4: a) Similar to Fig. 1(a) but from 23rd to 30th of August 2018. **b)** similar to Fig. 1(b) but for the period 23-30 of August 2018. **c)** similar to Fig. 1(c) but from 23 to 30 August 2018.

Figure 5: Percentage change in O/N2 from quiet time value at mid-latitudes (north in blue and south in red) region during the case of **a)** April 2012, **b)** March 2013, **c)** March 2015 and **d)** August 2018

Table 1

Case	Source	Min of SYM_H [nT]	Max AE index [nT]
23rd April 2012	CME	-125	1829
17th March 2013	CME+HSSW	-132	2690
17th March 2015	CME+HSSW	-234	2298
25th August 2018	CME+HSSW	-206	2100

Table 2

Case		April 2012	March 17 2013	March 17 2015	August 25 2018
Middle Latitudes	Magnetic quiet	σ_m=22 NH σ_m=14 SH	σ_m=18 NH σ_m=17 SH	σ_m=12 NH σ_m=15 SH	σ_m=14 NH σ_m=08 SH
	Main Phase	σ_m=18 NH **σ_m=32 SH**	**σ_m=36 NH** σ_m=17 SH	**σ_m=30 NH** **σ_m=40 SH**	σ_m=15 NH **σ_m=34 SH**
	Recovery phase	**σ_m=35 NH** **σ_m=45 SH**	**σ_m=52 NH** **σ_m=38 SH**	**σ_m=40 NH** **σ_m=42 SH**	**σ_m=38 NH** **σ_m=52 SH**
Low Latitudes	Magnetic quiet	σ_m=9 NH σ_m=10 SH	σ_m=06 NH σ_m=10 SH	σ_m=03 NH σ_m=05 SH	σ_m=06 NH σ_m=09 SH
	Main Phase	**σ_m=28 NH** σ_m=14 SH	σ_m=10 NH σ_m=18 SH	**σ_m=27 NH** σ_m=17 SH	**σ_m=26 NH** σ_m=15 SH
	Recovery phase	σ_m=9 NH σ_m=14 SH	σ_m=14 NH **σ_m=30 SH**	σ_m=15 NH **σ_m=25 SH**	**σ_m=31 NH** **σ_m=33 SH**

The authors declare that they have no conflict of interest

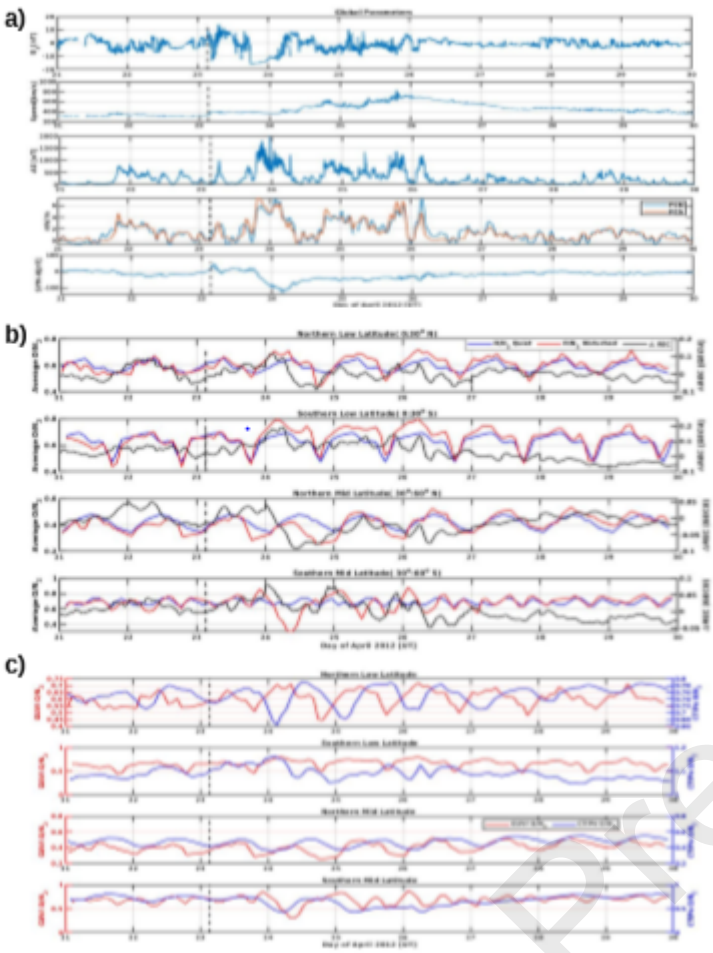

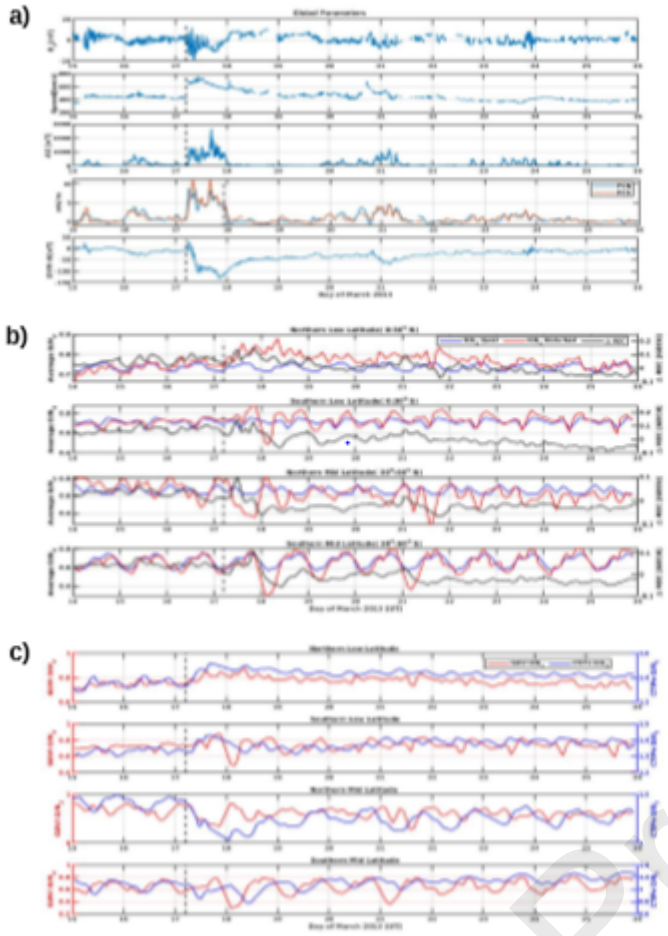

a)

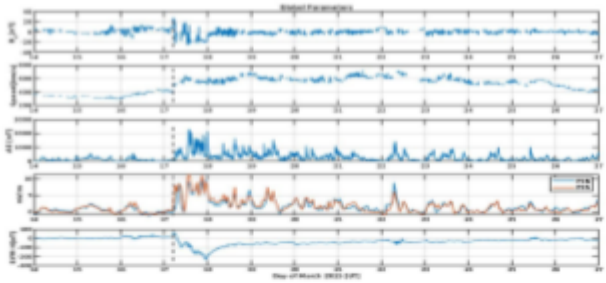

b)

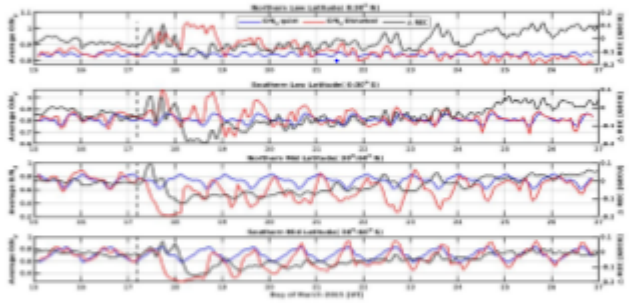

c)